

# **$B'$ 's with Direct Decays: Tevatron and LHC Discovery Prospects in the $b\bar{b}\cancel{E}_T$ Channel**

Johan Alwall,<sup>1</sup> Jonathan L. Feng,<sup>2</sup> Jason Kumar,<sup>3</sup> and Shufang Su<sup>2,4</sup>

<sup>1</sup>*Theoretical Physics Department, Fermi National Accelerator Laboratory,  
P.O. Box 500, Batavia, IL 60510, USA*

<sup>2</sup>*Department of Physics and Astronomy,  
University of California, Irvine, CA 92697, USA*

<sup>3</sup>*Department of Physics and Astronomy,  
University of Hawai'i, Honolulu, HI 96822, USA*

<sup>4</sup>*Department of Physics, University of Arizona, Tucson, AZ 85721, USA*

(Dated: July 2011)

## **Abstract**

We explore the discovery prospects for  $B'\bar{B}'$  pair production followed by direct decays  $B' \rightarrow bX$ , where  $B'$  is a new quark and  $X$  is a long-lived neutral particle. We develop optimized cuts in the  $(m_{B'}, m_X)$  plane and show that the 7 TeV LHC with an integrated luminosity of 1 (10)  $\text{fb}^{-1}$  may exclude masses up to  $m_{B'} \sim 620$  (800) GeV, completely covering the mass range allowed for new quarks that get mass from electroweak symmetry breaking. This analysis is applicable to other models with  $b\bar{b}\cancel{E}_T$  signals, including supersymmetric models with bottom squarks decaying directly to neutralinos, and models with exotic quarks decaying directly to GeV-scale dark matter. To accommodate these and other interpretations, we also present model-independent results for the  $b\bar{b}\cancel{E}_T$  cross section required for exclusion and discovery.

PACS numbers: 14.65.Jk, 13.85.Rm, 95.35.+d

## I. INTRODUCTION

This is an exciting time for TeV-scale colliders, with experiments at the Tevatron and Large Hadron Collider (LHC) collecting data at unprecedented luminosities and energies. In this study, we explore the prospects for discovering new physics through  $B'\bar{B}'$  production, followed by the direct decays  $B' \rightarrow bX$ , where  $B'$  is a new down-type quark (with electric charge  $q_{B'} = -\frac{1}{3}$ ) and  $X$  is a long-lived neutral particle, leading to the signal  $b\bar{b}\cancel{E}_T$ . This study complements our previous study of  $T'\bar{T}'$  production (where  $T'$  is an up-type quark with  $q_{T'} = \frac{2}{3}$ ), followed by the direct decay  $T' \rightarrow tX$ , leading to the signal  $t\bar{t}\cancel{E}_T$  [1].

The possibility of new physics leading to heavy flavor signals is, of course, well-appreciated, but such signals are usually accompanied by other visible particles from multi-step cascade decays. The direct decays considered here are much less studied, but are well-motivated from many perspectives. The gauge hierarchy problem, for example, motivates top and bottom partners, new particles that cancel the radiative contributions from bottom and top quark loops to the Higgs boson mass. The fine-tuning in such models is generally reduced when these partners are light, making it natural that such particles are among the lightest new particles and decay without cascades. The canonical example is supersymmetric models with top and bottom squarks that are lighter than the other squarks and decay directly through  $\tilde{b} \rightarrow b\chi_1^0$  and  $\tilde{t} \rightarrow t\chi_1^0$ , where  $\chi_1^0$  is the lightest neutralino.

Dark matter provides another general motivation for the signals we consider. In many models of dark matter, the dark matter particle  $X$  is the lightest particle charged under an exact symmetry, “dark charge,” and it may scatter off normal matter through processes  $Xq \rightarrow Q' \rightarrow Xq$ , where  $Q'$  is another new particle. This possibility is especially motivated at present by the possibility that such signals may in fact have been seen at DAMA [2], CoGeNT [3], and CRESST [4]. In such scenarios, the  $Q'$  particles are necessarily colored and have dark charge; they can be produced through  $q\bar{q}/gg \rightarrow Q'\bar{Q}'$  and decay directly through  $Q' \rightarrow qX$ . Although these decays may be to any quark flavor, decays to  $b$  and  $t$  are realized in concrete scenarios with WIMP dark matter, WIMPless dark matter, and asymmetric dark matter, as we review in Sec. II. Such models are also, of course, much more amenable to study at hadron colliders than those in which the decays are solely to light quarks.

In a previous study [1], we investigated the collider reach for up-type quark pair production  $q\bar{q}/gg \rightarrow T'\bar{T}'$ , followed by  $T' \rightarrow tX$ . In this work, we analyze the pair production of down-type quark  $B'\bar{B}'$  with subsequent decay of  $B' \rightarrow bX$  at both the Tevatron and 7 TeV LHC using the Madgraph/MadEvent/Pythia/PGS4 packages. For relatively small values of  $m_X$ , we will find that  $B'$  masses up to 440, 460 and 480 GeV may be excluded given integrated luminosities of 5, 10, and 20 fb<sup>-1</sup> at the Tevatron, respectively. This reach is greatly enhanced at the 7 TeV LHC: with an integrated luminosity of only 100 pb<sup>-1</sup>, the 7 TeV LHC’s 95% CL exclusion reach is comparable to that of the Tevatron with 20 fb<sup>-1</sup>. The whole region of  $m_{B'}$  allowed by Yukawa coupling perturbativity can be explored with 1 fb<sup>-1</sup> of data, and, with 10 fb<sup>-1</sup> of data,  $B'$  masses up to 800 GeV may be excluded. The 7 TeV LHC also has great potential in terms of  $B'$  discovery:  $3\sigma$  discovery contours reach  $B'$  masses of 540 and 700 GeV for integrated luminosities of 1 and 10 fb<sup>-1</sup>, respectively.

We also present model-independent results for collider reaches as a function of the  $bX\bar{b}X$  production cross-section, with  $m_X = 1$  GeV. From these, for any theoretical prediction for  $\sigma(B'\bar{B}') \times B(B' \rightarrow bX)^2$  as a function of  $m_{B'}$ , one can easily determine the expected exclusion and discovery reaches in  $m_{B'}$ . Our results may therefore be applied to other models

that give rise to the  $b\bar{b}\cancel{E}_T$  signal.

In Sec. II, we discuss models that yield the  $b\bar{b}\cancel{E}_T$  signal and their implications for the  $B'$  and  $X$  masses. In Sec. III we discuss existing bounds on these scenarios. Our simulation is described in Sec. IV. The results are presented in Sec. V and summarized in Sec. VI. In the Appendix, we list cross sections at the Tevatron and 7 TeV LHC for standard model (SM) backgrounds and several benchmark points after various levels of cuts.

## II. MODELS

We now discuss models that yield the  $b\bar{b}\cancel{E}_T$  signal and their implications for the  $B'$  and  $X$  masses. We begin with the familiar examples of supersymmetry and universal extra dimensions (UED), where the spins of the  $B'$  and  $X$  particles are  $(S_{B'}, S_X) = (0, \frac{1}{2})$  and  $(\frac{1}{2}, 1)$ , respectively. These are model frameworks in which existing searches have been carried out and the  $X$  particle is WIMP dark matter. We then discuss models with WIMPlless and asymmetric dark matter, where the spins are  $(S_{B'}, S_X) = (\frac{1}{2}, 0)$ . In these models,  $X$  is again dark matter, but the light mass range  $m_X \sim 1\text{--}10$  GeV is particularly motivated by currently claimed signals. Strictly speaking, our analysis is valid only for the spin assignment of the WIMPlless and asymmetric dark matter cases, but as described below, it is also applicable to the other scenarios with minor modifications.

### A. Supersymmetry with Light Bottom Squarks

Supersymmetric models yield the  $b\bar{b}\cancel{E}_T$  signal when bottom squark pair production is followed by direct decays  $\tilde{b} \rightarrow b\chi_1^0$ , where  $\chi_1^0$  is the lightest neutralino, an excellent dark matter candidate [5, 6]. Squarks are often assumed to decay through cascade decay chains. In contrast to other squarks, however, bottom (and top) squarks have their masses reduced by the impact of large Yukawa couplings on renormalization group evolution, and their masses are also directly constrained by naturalness. There are therefore reasons to expect the bottom squarks to be relatively light and decay directly to the lightest supersymmetric particle, even if other squarks are heavy and decay through cascades.

The salient features for this analysis are

- The signal arises from bottom squark pair production followed by  $\tilde{b} \rightarrow b\chi_1^0$ . The decaying particle is a scalar, in contrast to all other examples discussed below.
- The  $\tilde{b}$  mass is only constrained by direct searches discussed in Sec. III, which require  $m_{\tilde{b}} \gtrsim 230$  GeV for small  $m_{\chi_1^0}$ . The mass limit on  $m_{\tilde{b}}$  becomes much weaker for small mass splitting  $m_{\tilde{b}} - m_{\chi_1^0}$ .
- The neutralino mass satisfies  $m_{\chi_1^0} \gtrsim 47$  GeV, assuming gaugino mass unification [7]. Without gaugino mass unification, there is no lower bound on the neutralino mass, which in general may be anywhere in the range  $0 \lesssim m_{\chi_1^0} < m_{\tilde{b}}$ .

### B. Universal Extra Dimensions

UED models give the desired signature, where the new down-type quark  $B'$  is identified with the Kaluza-Klein bottom quark  $b^1$ . The  $b^1$  can be pair-produced and then decay directly to Kaluza-Klein hypercharge gauge bosons  $B^1$ , which may be WIMP dark matter [8, 9].

The salient features of this model are

- The signal arises from  $b^1$  pair production followed by  $b^1 \rightarrow bB^1$ .
- The  $b^1$  mass is set by the size of the extra dimension. Its mass is constrained only by the direct searches discussed in Sec. III, which require  $m_{b^1} \gtrsim 440$  GeV for small  $m_{B^1}$ . If  $m_{B^1} \approx m_{b^1}$ , the mass limit is much weaker.
- The size of the extra dimension typically sets the size of all the Kaluza-Klein particles, and so UED spectra are typically expected to be compressed relative to supersymmetry. One therefore expects  $m_{B^1} \sim m_{b^1}$ , but  $B^1$  masses anywhere in the range  $0 \lesssim m_{B^1} < m_{b^1}$  are experimentally viable.

### C. WIMPless Dark Matter

In WIMPless scenarios [10], dark matter is in a hidden sector. These scenarios have the notable feature that the dark matter candidate automatically has approximately the correct relic density, regardless of the candidate particle’s mass.

The WIMPless dark matter particle  $X$  couples SM quarks to new quarks through Yukawa interactions

$$V = \lambda_i^q X \bar{Q}'_L q_{Li} + \lambda_i^u X \bar{T}'_R u_{Ri} + \lambda_i^d X \bar{B}'_R d_{Ri} , \quad (1)$$

where  $X$  is assumed here to be a complex scalar charged under a discrete symmetry,  $q_{Li}^T = (u_{Li}, d_{Li})$ ,  $u_{Ri}$ , and  $d_{Ri}$  are the SM quarks of generation  $i$ , and  $Q'^T_L = (T'_L, B'_L)$ ,  $T'_R$ , and  $B'_R$  are the new quarks, also charged under the same discrete symmetry as  $X$ .

In general, the Yukawa couplings can couple  $X$  to any of the SM generations, subject to flavor constraints [11]. Although it is difficult to know what a “natural” flavor structure for new quark couplings should be, one reasonable possibility is that new quark couplings follow the observed Yukawa hierarchy and couple new quarks dominantly to third generation quarks. In fact, for  $\mathcal{O}(1)$  Yukawa couplings, WIMPless models with dark matter coupled to 3rd generation quarks may explain the reported dark matter signals from DAMA and CoGeNT [12].

For the purpose of the analysis presented here, the salient features are

- The signal arises from  $B'$  pair production followed by the decay  $B' \rightarrow bX$ . Dark charge conservation forbids the cascade decays  $B' \rightarrow Wq$  and  $B' \rightarrow Zq$ , and the possibilities  $B' \rightarrow dX, sX$  are excluded by hand.
- $T'$  and  $B'$  are new quarks that get mass through electroweak symmetry breaking, with  $m_{T',B'} = \lambda_{T',B'} v / \sqrt{2}$ , where  $v \simeq 246$  GeV. Yukawa coupling perturbativity requires  $\lambda_{B'}^2 \lesssim 4\pi$ , which implies the upper bound  $m_{B'} \lesssim 600$  GeV. For small  $m_X$ , direct searches [13–15] place a lower bound,  $m_{B'} \gtrsim 440$  GeV. This lower bound is weakened for larger dark matter mass.
- For  $X$  to freeze out with the correct relic density and preserve a key motivation for WIMPless scenarios, it cannot be extremely light, but the range  $10 \text{ MeV} \lesssim m_X < m_{B'}$  is allowed. However, if one hopes to explain the DAMA [2] and CoGeNT [3] anomalies and be marginally consistent with stringent exclusion bounds from CDMS [16] and XENON10/100 [17], light masses with  $m_X \sim 7$  GeV are preferred.

There are several other models that share the basic features described above. One well-known example is little Higgs models, where the new quarks are not 4th generation quarks,

but instead arise from the extra degrees of freedom needed when the gauge symmetry  $SU(2)_L$  is enlarged. Unlike the WIMPless case, the mass of the new quarks is not generated by Yukawa couplings to the SM Higgs, and thus is not bounded from above by perturbativity. These quarks may also be charged under  $T$ -parity, decaying to SM quarks plus dark matter (the lightest particle charged under  $T$ -parity) [18]. Another example is provided by a recent set of models in which  $U(1)_B$  is a gauge symmetry [19]. In this case, the new quarks are 4th generation (possibly mirror) quarks that are added to cancel the  $U(1)_B$  mixed anomaly. They are charged under a new  $U(1)$  global symmetry, and the dark matter is a scalar which is the lightest particle charged under this global  $U(1)$ .

#### D. Asymmetric Dark Matter

Another class of models predicting the  $b\bar{b}\cancel{E}_T$  signature are models of asymmetric dark matter arising from hidden sector baryogenesis [20]. In this framework, sphalerons of a hidden sector gauge group generate a baryon asymmetry by producing exotic quarks [21]. The  $B'$  is the down-type exotic quark, which decays to dark matter and right-handed bottom quarks,  $B' \rightarrow b_R X$ . Our analysis is directly applicable when the dark matter particle is a scalar.<sup>1</sup> In this model, the number density of the dark matter candidate is determined by the baryon number density. Moreover, the dark matter multiplet and  $b$ -quark multiplet are both chiral under a  $U(1)_{T3R}$  gauge group; both  $m_X$  and  $m_b$  are determined by the symmetry-breaking scale of  $U(1)_{T3R}$ , so one expects  $m_X \sim m_b$ . As a result, this asymmetric dark matter candidate naturally has approximately the correct relic density.

For the purposes of this analysis, the salient features of the asymmetric dark matter model are

- The exotic down-type quark  $B'$  is not a 4th generation quark, and its mass is not generated by electroweak symmetry breaking. As a result, there is no upper bound on its mass, which is only constrained by direct searches to satisfy  $m_{B'} \gtrsim 440$  GeV for small  $m_X$ .
- The asymmetric dark matter should have  $m_X \sim 1 - 10$  GeV to correctly explain the relic density. But a dark matter mass  $m_X \sim 7$  GeV is preferred to explain reported direct detection signals.
- The exotic quark need not be down-type, but if it is, it necessarily decays through  $B' \rightarrow bX$ .

### III. CURRENT COLLIDER LIMITS

In this section, we summarize existing constraints on the  $b\bar{b}\cancel{E}_T$  signature and related channels. All bounds quoted below are 95% CL constraints.

As noted in Sec. I, we are interested in  $B'\bar{B}'$  production followed by direct decays  $B' \rightarrow bX$ . These differ from searches for conventional fourth generation quarks, which we denote by the lowercase  $b'$  and  $t'$ , which typically decay through cascades. Nevertheless, we begin with these as a useful reference point. Searches for  $t'$  and  $b'$  has been performed at both

---

<sup>1</sup> In general, the dark matter candidate can also be spin- $\frac{1}{2}$  for this model. In this case, the relevant signal is pair production of the down-type exotic squark,  $\tilde{B}'$ , followed by the decay  $\tilde{B}' \rightarrow b_R X$ .

Run II of the Tevatron [22–25] and the LHC [26, 27]. These searches assume that the fourth generation quarks couple to the first three generations and decay through  $b', t' \rightarrow qW$ . For  $b'$ , the most stringent result at present is from CDF searches for  $b'\bar{b}'$  production followed by  $b' \rightarrow tW$ . The lack of an excess in  $4.8 \text{ fb}^{-1}$  of data implies  $m_{b'} > 372 \text{ GeV}$  [23]. For  $t'$ , CDF finds no signal for  $t'\bar{t}'$  production followed by  $t' \rightarrow bW$  in  $5.6 \text{ fb}^{-1}$  of data, implying  $m_{t'} > 358 \text{ GeV}$  [24], and a DØ search for  $t'\bar{t}'$  followed by  $t' \rightarrow qW$  in  $4.3 \text{ fb}^{-1}$  of data requires  $m_{t'} > 296 \text{ GeV}$  [25]. At the LHC, null results from CMS searches for  $b' \rightarrow tW$  using  $34 \text{ pb}^{-1}$  of data imply  $m_{b'} > 361 \text{ GeV}$  [26]. ATLAS analyses of  $t'$  or  $b' \rightarrow qW$  in  $37 \text{ pb}^{-1}$  of data imply  $m_{t', b'} > 270 \text{ GeV}$  [27]. We stress again, however, that the limits of this paragraph do not apply to the  $B'$  and  $T'$  searches we consider here, as decays  $B' \rightarrow qW$  and  $T' \rightarrow qW$  are excluded by dark charge conservation.

As noted in Sec. II A, however, the  $b\bar{b}\cancel{E}_T$  signal is produced in the case of supersymmetry with bottom squark pair production followed by  $\tilde{b} \rightarrow b\chi_1^0$ , where  $\chi_1^0$  is the lightest neutralino. Both CDF and DØ have searched for this signal. DØ finds no excess in  $5.2 \text{ fb}^{-1}$  of data, requiring  $m_{\tilde{b}} > 247 \text{ GeV}$  for  $m_{\chi_1^0} = 0$  and excluding  $160 \text{ GeV} < m_{\tilde{b}} < 200 \text{ GeV}$  for  $m_{\chi_1^0} = 110 \text{ GeV}$  [13]. The corresponding CDF result for  $m_{\chi_1^0} = 0$  using  $2.65 \text{ fb}^{-1}$  of data is  $m_{\tilde{b}} > 230 \text{ GeV}$  [14]. Taking into account only the difference in  $B'\bar{B}'$  and  $\tilde{b}\tilde{b}^*$  cross sections, the DØ bound  $m_{\tilde{b}} > 247 \text{ GeV}$  implies  $m_{B'} \gtrsim 365 \text{ GeV}$ . As we will see in Sec. V, an optimized collider analysis would imply  $m_{B'} \gtrsim 440 \text{ GeV}$  when cuts similar to those of the DØ sbottom searches are applied to  $B'\bar{B}'$  pair production. Signal significance would be reduced by a trials factor associated with the choice of optimum cuts, however.

A search for gluino pair production with  $\tilde{g} \rightarrow \tilde{b}\tilde{b}$  followed by  $\tilde{b} \rightarrow b\chi_1^0$  has been carried out at CDF using an integrated luminosity of  $2.5 \text{ fb}^{-1}$  [15]. Candidate events were selected requiring two or more jets, large  $\cancel{E}_T$ , and at least two  $b$ -tags. Using neural net analyses, CDF found  $m_{\tilde{g}} > 350 \text{ GeV}$  for large mass splittings  $\Delta m \equiv m_{\tilde{g}} - m_{\tilde{b}} \gtrsim 80 \text{ GeV}$ , and about  $340 \text{ GeV}$  for small  $\Delta m \sim 20 \text{ GeV}$ . The result for the case of small  $\Delta m$ , where two  $b$ -jets are soft and sometimes missed, can be applied to the  $B'\bar{B}'$  search and imply roughly  $m_{B'} \gtrsim 370 \text{ GeV}$ .

SUSY searches by the ATLAS Collaboration at the LHC with  $\sqrt{s} = 7 \text{ TeV}$  and  $35 \text{ pb}^{-1}$  luminosity [28] studied the process of gluino and sbottom pair production with  $\tilde{g} \rightarrow \tilde{b}\tilde{b}_1$  and  $\tilde{b}_1 \rightarrow b\chi_1^0$ . Events are selected by requiring large  $\cancel{E}_T$  and at least three jets, of which at least one is  $b$ -tagged. For  $m_{\tilde{b}_1} < 500 \text{ GeV}$ , this search implies  $m_{\tilde{g}} > 590 \text{ GeV}$ . This limit also bounds  $B'\bar{B}' \rightarrow \tilde{b}\tilde{b}_1\cancel{E}_T$ , where the additional jet results from QCD radiation. It is, however, not straightforward to obtain the mass limit on  $m_{B'}$  without detailed collider analyses.

Although we focus here on  $B'$  production, if the  $B'$  mass is generated by electroweak symmetry breaking then the mass difference between  $B'$  and  $T'$  is constrained by electroweak precision data to be less than about  $50 \text{ GeV}$  [29]. Therefore, bounds on  $T'$  production are also relevant. The discovery prospects for  $T'\bar{T}'$  production followed by direct decays were evaluated in Ref. [1], and we summarize current bounds here.

A CDF search for  $T'\bar{T}' \rightarrow t\bar{t}\cancel{E}_T$  in the semi-leptonic channel in  $4.8 \text{ fb}^{-1}$  of data implies  $m_{T'} > 360 \text{ GeV}$  for  $m_X \leq 100 \text{ GeV}$  [30]. SUSY searches for stop pair production at the Tevatron followed by  $\tilde{t} \rightarrow b\ell\tilde{\nu}$  also imply bounds on  $T'\bar{T}' \rightarrow t\bar{t}\cancel{E}_T$  when both tops decay leptonically. Null results from searches at both CDF [31] and DØ [32] in  $1 \text{ fb}^{-1}$  of data imply  $m_{\tilde{t}} \gtrsim 180 \text{ GeV}$  for  $m_{\tilde{\nu}} \lesssim 100 \text{ GeV}$ . Accounting for the difference in  $\tilde{t}\tilde{t}^*$  and  $T'\bar{T}'$  cross sections, this implies the bound  $m_{T'} \gtrsim 263 \text{ GeV}$ . The CDF Collaboration has also reported a search for top squark pair production based on an integrated luminosity of  $2.7 \text{ fb}^{-1}$ , using the purely leptonic final states from  $p\bar{p} \rightarrow \tilde{t}_1\tilde{t}_1^*$ , followed by  $\tilde{t}_1 \rightarrow b\chi_1^\pm \rightarrow b\ell\nu\chi_1^0$  [33]. The data are consistent with the SM background, leading to the constraint  $m_{\tilde{t}_1} \gtrsim 150 - 185 \text{ GeV}$ ,

where the exact limit depends on  $m_{\chi_1^0}$ ,  $m_{\chi_1^\pm}$ , and  $B(\chi_1^\pm \rightarrow l^\pm \nu \chi_1^0)$ .

Stop pair production (either direct or via gluino decay  $\tilde{g} \rightarrow t\bar{t}_1$ ) has been searched for at ATLAS with  $\sqrt{s} = 7$  TeV and  $35 \text{ pb}^{-1}$  [28]. Assuming  $B(\tilde{t}_1 \rightarrow b\chi_1^\pm) = 1$  and  $B(\chi_1^\pm \rightarrow \chi_1^0 W^{(*)}) = 1$ , searches have been performed in the semi-leptonic channel with 1 lepton, 2 jets (including one  $b$ -jet) and large  $\cancel{E}_T$ . For  $130 \text{ GeV} < m_{\tilde{t}} < 300 \text{ GeV}$ , this search implies  $m_{\tilde{g}} > 520 \text{ GeV}$ . Cross sections for  $\tilde{g}\tilde{g} + \tilde{t}_1\tilde{t}_1^*$  around 8 to 40 pb have been excluded for  $400 \text{ GeV} < m_{\tilde{g}} < 600 \text{ GeV}$ . It is less straightforward to translate this search limit to the  $T'$  case, given the very different cut efficiencies of the dominant  $\tilde{g}\tilde{g}$  process.

Finally, a recent search at ATLAS with  $\sqrt{s} = 7$  TeV and  $35 \text{ pb}^{-1}$  [34] for pair production of fermionic top partners decaying to a top quark and a long-lived neutral particle gives a mass limit of  $m_{T'} > 275$  (300) GeV for  $m_X < 50$  (10) GeV. This limit can be directly applied to the case of  $T'$  pair production followed by direct decays.

## IV. COLLIDER ANALYSIS

### A. Signal and background simulation

Both signal and backgrounds were simulated using MadGraph/MadEvent 4 [35] and passed through Pythia 6.4 [36] (with  $p_T$ -ordered showers) for parton showering and hadronization. We used the CTEQ6L1 parton distribution functions [37] and the factorization and renormalization scales were set to  $m^2 + p_T^2$  of the massive particles produced. Detectors were simulated with PGS4 [38] using the Tevatron and ATLAS detector cards for Tevatron and LHC simulations, respectively, as provided by MadGraph/MadEvent.

Our signal process is  $pp/p\bar{p} \rightarrow B'\bar{B}' + \text{jets}$  with  $B' \rightarrow bX$ , using matrix elements with jet matching for up to 2 jets and the decay at matrix element level, giving a signal of two  $b$ -jets and missing energy, plus possible associated jets from QCD radiation. We generated events at grid points in the  $(m_{B'}, m_X)$  plane with 25,000 events per grid point.

The main backgrounds to this process are  $W^\pm + \text{jets}$ ,  $Z + \text{jets}$ , and  $t\bar{t}$  production. The former two were simulated with up to 3 jets coming from the matrix element and the latter with up to 1 jet from the matrix element, to ensure that the backgrounds were properly modeled with respect to the jet cuts used in the analyses. Also the single top background and diboson background were simulated and found to be negligible, as expected. The backgrounds have been compared to similar Tevatron [39] and ATLAS [40–42] analyses, with agreement at the expected 20% level. The exception is  $b$ -tagging, where the experimental efficiency for the Tevatron DØ detector is better than that given by PGS. We have therefore applied a correction factor to our Tevatron  $b$ -tagging efficiency to reproduce the efficiencies quoted in the experimental analyses.

The choice of cuts to distinguish signal from background is guided by a few key features. SM backgrounds exhibit  $\cancel{E}_T$  either because of neutrino production or jet energy mismeasurement. The first source is suppressed by a lepton veto, which rejects processes involving  $W \rightarrow \ell\nu$ . The second source can be effectively suppressed by a combination of minimum  $\cancel{E}_T$  cuts (which suppress multi-jet backgrounds) and the requirement that  $\cancel{E}_T$  not be aligned with any energetic jets. The alignment cut is imposed in terms of a minimum angle between the missing transverse energy and any of the selected jets,  $\Delta\phi_{\min}(\cancel{E}_T, \text{jets})$ . Since  $\cancel{E}_T$  can also be mismeasured in events with significant transverse momentum in low-energy jets and leptons, such events can be removed by cuts on the quantity  $\mathcal{A} \equiv (\cancel{E}_T - \cancel{H}_T)/(\cancel{E}_T + \cancel{H}_T)$ ,

where  $\cancel{E}_T \equiv |\sum_{\text{jets}} \vec{p}_T^j|$  is the magnitude of the vector sum of the transverse energy of all jets.

Moreover, signal events result in the pair production of two massive objects, whose decays to  $b$ -jets and invisible particles are roughly uncorrelated. These events are thus expected to have several objects with large  $p_T$ , with most of the transverse momentum carried by the two leading jets, which are not expected to be back-to-back. The  $\cancel{E}_T$  is also expected to be comparable to the  $p_T$  of the other objects. For the Tevatron, the presence of objects with large  $p_T$  is measured by the kinematic variable  $H_T \equiv \sum_{\text{jets}} p_T^j$ , while at the LHC it is measured by the kinematic variable  $M_{\text{eff}} = \cancel{E}_T + \sum_{j_1 \dots j_4} p_T^j$ .

At the Tevatron, the requirement that the leading jets not be back-to-back is measured by the kinematic variable  $\alpha_{j_1 j_2}$ , defined as the angle between the two leading jets in the transverse plane. At the LHC this requirement is imposed in terms of the transverse sphericity,  $S_T$ . If  $\lambda_{1,2}$  are the eigenvalues of the  $2 \times 2$  sphericity tensor  $S_{ij} = \sum_k p_{ki} p_{kj}$  for all selected jets, one defines  $S_T \equiv 2\lambda_2/(\lambda_1 + \lambda_2)$ . QCD backgrounds are dominated by back-to-back jet configurations, for which  $S_T \sim 0$ .

At the Tevatron, the requirement that most transverse momenta be carried by the two leading jets is measured by the kinematic variable  $X_{jj} \equiv (p_T^{j_1} + p_T^{j_2})/H_T$ . At the LHC, the requirement that the missing transverse energy be comparable to the momenta of other objects is measured in terms of  $f \equiv \cancel{E}_T/M_{\text{eff}}$ .

Note that we have chosen not to take into account next-to-leading order  $K$  factors in our analysis. We consider this conservative, in the sense that next-to-leading calculations tend to increase signal and background (both QCD and vector boson + jets) with a similar factor ( $\sim 1.2 - 1.5$ ), and therefore tend to increase the significance of the result and improve the exclusion and discovery regions [43, 44].

## B. Tevatron Cuts

For Tevatron searches, we begin by imposing precuts that are similar to the cuts required in Ref. [39] for sbottom searches. With these precuts, we require:

- 0 lepton with  $|\eta_\ell| \leq 2.0$  and  $p_T^{e,\mu} \geq 15$  GeV and  $p_T^\tau \geq 10$  GeV.
- 2 or 3 jets with  $|\eta_j| \leq 2.5$  and  $p_T^j \geq 20$  GeV.
- $\alpha_{j_1 j_2} \leq 165^\circ$ .
- $\cancel{E}_T \geq 40$  GeV,  $\cancel{E}_T/\text{GeV} \geq 80 - 40 \times \Delta\phi_{\min}(\cancel{E}_T, \text{jets})$ .
- At least two jets, including the leading jet, are tagged as  $b$ -jets.
- $\Delta\phi_{\min}(\cancel{E}_T, \text{jets}) \geq 0.6$  rad.
- $-0.1 < \mathcal{A} < 0.2$ .
- $X_{jj} \geq 0.75$ .

In addition, for each grid point in  $(m_{B'}, m_X)$  space, we consider the following cuts and choose the combination that optimizes the signal's significance:

- $p_T^{j_1} \geq 50, 80, 100, 150$  GeV.
- $\cancel{E}_T \geq 100, 150, 200, 250$  GeV.
- $X_{jj} \geq 0.9$ .
- $H_T \geq 150, 220, 300$  GeV.

Note that some of the final cut combinations are redundant (e.g.,  $H_T < p_T^{j_1} + p_T^{j_2}$ ), resulting in a total of 160 naively non-redundant combinations.

Comparing our cut efficiencies for sbottom pair production with those listed in Ref. [39] for two signal benchmark points  $(m_{\tilde{b}_1}, m_{\chi_1^0}) = (240 \text{ GeV}, 0 \text{ GeV})$  and  $(130 \text{ GeV}, 85 \text{ GeV})$ , we found reasonably good agreement, except for the  $b$ -tagging efficiency for two jets, which was underestimated by about a factor of 2 in PGS4. We therefore increase our cut efficiencies by a factor of two (for both the signal process and the  $t\bar{t}$  background) to account for this underestimation caused by our using PGS4 for detector simulation.

### C. LHC Cuts

For the LHC, we adopt the following precuts based on the cuts designed for inclusive SUSY searches for 0 lepton, 2–3 jets (including 1–2  $b$ -jets) at the LHC [40–42]:

- 0 lepton with  $|\eta_{e,\mu,\tau}| \leq 2.5$  and  $p_T^{e,\mu,\tau} \geq 20 \text{ GeV}$ .
- 2 or 3 jets with  $|\eta_j| \leq 2.5$  and  $p_T^{j_1} \geq 100 \text{ GeV}$ ,  $p_T^{j_{2,3}} \geq 40 \text{ GeV}$ ,  $p_T^{j(\text{veto})} = 30 \text{ GeV}$ .
- $\cancel{E}_T \geq 80 \text{ GeV}$ .
- $f \equiv \cancel{E}_T/M_{\text{eff}}$ ,  $f \geq 0.3$  (0.25) for 2-jet (3-jet) events.
- $\Delta\phi_{\min}(\cancel{E}_T, \text{jets}) \geq 0.2 \text{ rad}$  for all selected jets.
- Transverse sphericity  $S_T \geq 0.2$ .
- At least one selected jet is tagged as a  $b$ -jet.

The cuts on the transverse momentum of jets are chosen to satisfy the trigger requirements, as well as to reject a sufficient amount of QCD jet background.

In addition, for each grid point in  $(m_{B'}, m_X)$  space, we consider the following cuts and choose the combination that optimizes the signal's significance:

- $p_T^{j_1} \geq 150, 200, 250, 300 \text{ GeV}$ .
- $\cancel{E}_T \geq 100, 150, 200, 250, 300 \text{ GeV}$ .
- $M_{\text{eff}} \geq 250, 300, 400, 500, 600, 700 \text{ GeV}$ .

Note that some of these final cut combinations are redundant (e.g., when  $M_{\text{eff}} < p_T^{j_1} + p_T^{j_2} + \cancel{E}_T$ ), resulting in a total of 104 non-redundant combinations.

## V. RESULTS AND DISCUSSION

Figure 1 shows the  $\cancel{E}_T$  and  $H_T$  distributions for three benchmark points  $(m_{B'}, m_X) = (200, 1), (300, 1), (400, 1) \text{ GeV}$  as well as the dominant SM backgrounds at the Tevatron after precuts.  $W(\ell\nu)jj$  becomes the dominant background after precuts, and  $Z(\nu\nu)jj$  and semileptonic  $t\bar{t}$  background are relatively large as well. While the differential cross section distributions for the SM backgrounds drop quickly with increasing  $\cancel{E}_T$  and  $p_T^{j_1}$ , the distributions for the signal typically extends to much larger values of  $\cancel{E}_T$  and  $H_T$ , given the relatively large mass splittings between  $m_{B'}$  and  $m_X$ . As a result, additional cuts on  $\cancel{E}_T$  and  $H_T$  (as well as  $p_T^{j_1}$  and  $X_{jj}$ ) can effectively suppress the backgrounds while keeping most of the signal intact, thereby optimizing the signal significance.

Similarly,  $p_T^{j_1}$  and  $M_{\text{eff}}$  distributions at the 7 TeV LHC after precuts are shown in Fig. 2 for three benchmark points  $(m_{B'}, m_X) = (300, 1), (500, 1), (800, 1) \text{ GeV}$ , as well as the

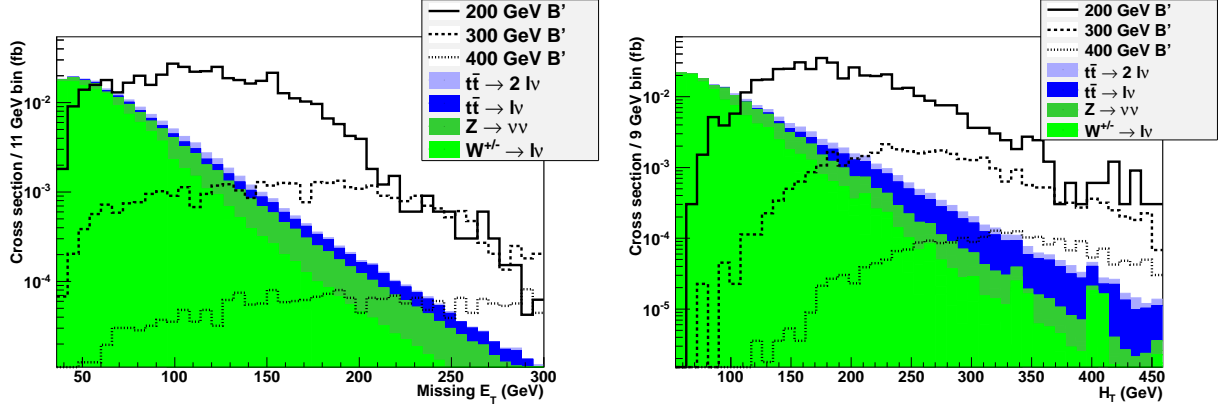


FIG. 1:  $\cancel{E}_T$  and  $H_T$  distributions at the Tevatron for SM backgrounds and three signal benchmark points  $(m_{B'}, m_X) = (200, 1), (300, 1), (400, 1)$  GeV, after precuts.

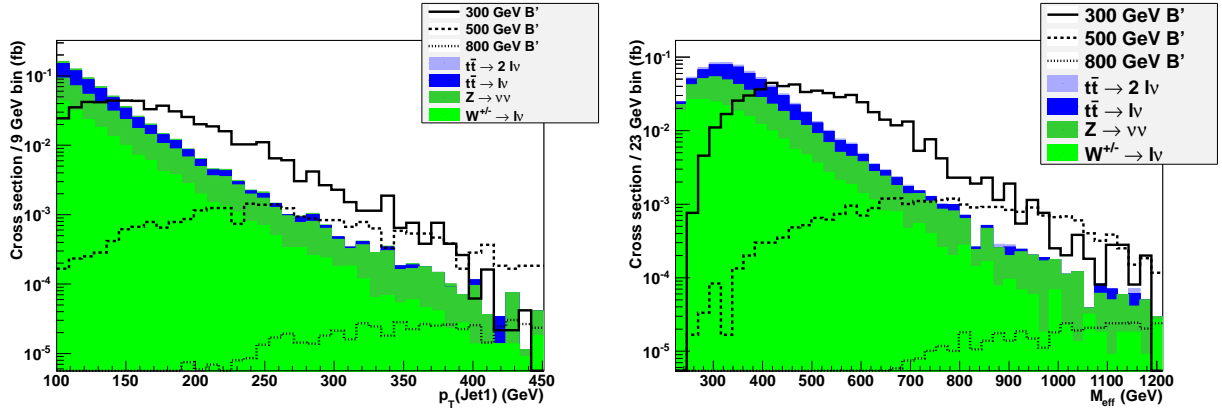


FIG. 2:  $p_T^{j_1}$  and  $M_{\text{eff}}$  distributions at 7 TeV LHC for SM backgrounds and three signal benchmark points  $(m_{B'}, m_X) = (300, 1), (500, 1), (800, 1)$  GeV, after precuts.

dominant SM backgrounds. The contributions from  $Z(\nu\nu)jj$ ,  $W(\ell\nu)jj$  and  $t\bar{t}$  are similar after precuts. However, for  $t\bar{t}$ , the differential cross section distributions drop quickly with increasing  $\cancel{E}_T$ ,  $p_T^{j_1}$  and  $M_{\text{eff}}$ , since the  $t\bar{t}$  distributions are enhanced in the region below the  $t$  mass (for  $\cancel{E}_T$  and  $p_T^{j_1}$ ) and  $2m_t$  (for  $M_{\text{eff}}$ ). With additional cuts on  $\cancel{E}_T$ ,  $p_T^{j_1}$  and  $M_{\text{eff}}$ , the  $t\bar{t}$  background is almost negligible. The  $Z(\nu\nu)jj$  background, on the other hand, becomes dominant once additional cuts are imposed. For the signal benchmark point  $(m_{B'}, m_X) = (300, 1)$  GeV, the distributions drop quickly above the mass scale of the  $B'$ . To optimize the cuts for such low  $m_{B'}$ , usually no additional  $\cancel{E}_T$  or  $p_T^{j_1}$  cuts are needed and the  $M_{\text{eff}}$  cut becomes the most effective in selecting the signal. For larger masses, the  $p_T^{j_1}$  and  $\cancel{E}_T$  cuts become very effective in suppressing the backgrounds. The cross sections for signal benchmark points and SM backgrounds after various stages of cuts are presented in the Appendix.

We now determine the discovery and exclusion reach for  $B'$  at the Tevatron and the 7 TeV LHC. For each parameter point  $(m_{B'}, m_X)$ , we use the optimum cut (after precuts) that gives the best signal significance, with the additional requirements that  $S/B > 0.1$  and more than two signal events are observed. Given the small number of signal and background events after cuts, we have used Poisson statistics, rather than assuming Gaussian distributions, for

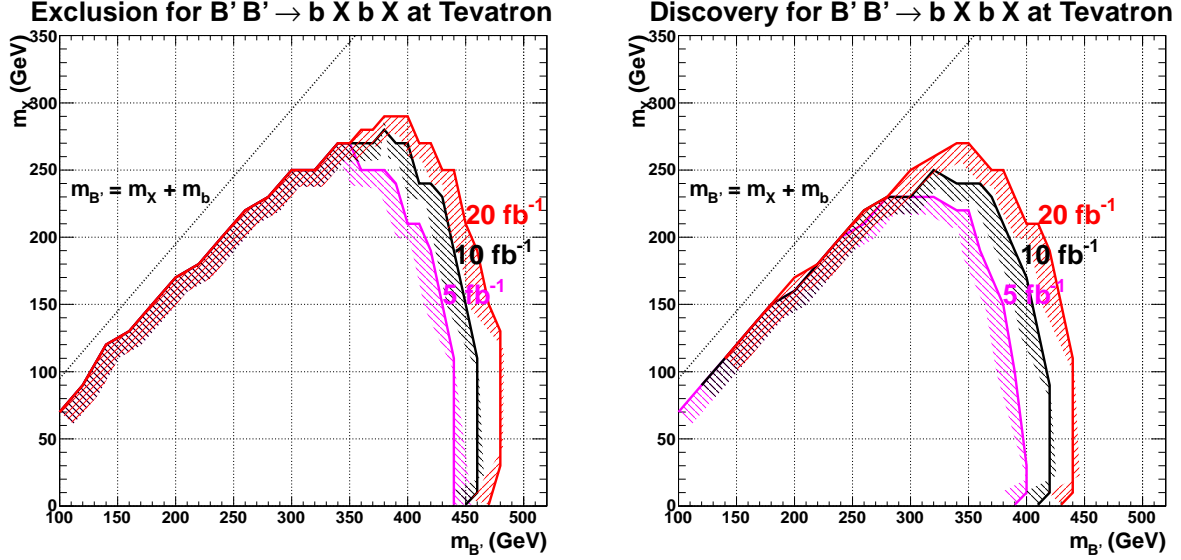


FIG. 3: 95% CL Tevatron exclusion (left plot) and  $3\sigma$  discovery (right plot) reach in the  $(m_{B'}, m_X)$  plane for integrated luminosities 5, 10, and  $20 \text{ fb}^{-1}$ . For each point in parameter space, the cut with the best significance has been chosen.

both signal and backgrounds.

Figure 3 shows the 95% CL Tevatron exclusion and  $3\sigma$  (Gaussian equivalent<sup>2</sup>) discovery contours in the  $(m_{B'}, m_X)$  plane. For relatively small values of  $m_X$ ,  $m_{B'}$  could be excluded up to 440, 460 and 480 GeV, or could be discovered at  $3\sigma$  up to 400, 420 and 440 GeV for integrated luminosities of 5, 10, and  $20 \text{ fb}^{-1}$ , respectively. For small mass splittings  $m_{B'} - m_X$ , the  $b$ -jets become soft and the amount of transverse missing energy gets smaller. It is more challenging to select signals out of the SM backgrounds with such soft decay products. This explains the gap between the exclusion/discovery contours and the dashed line, which corresponds to the threshold for the on-shell decay of  $B' \rightarrow bX$ . With  $20 \text{ fb}^{-1}$  integrated luminosity, masses  $m_X$  as large as 290 GeV may be excluded, and masses  $m_X$  as large as 270 GeV may be discovered.

Figure 4 shows the 95% CL exclusion and  $3\sigma$  (Gaussian equivalent) discovery contours for a 7 TeV early LHC run, for integrated luminosities 0.1, 1, and  $10 \text{ fb}^{-1}$ . With just  $0.1 \text{ fb}^{-1}$ , the LHC exclusion reach for  $m_{B'}$  of 480 GeV exceeds the Tevatron exclusion reach with  $20 \text{ fb}^{-1}$  luminosity. With  $1 \text{ fb}^{-1}$  and  $m_X \sim 0$ , all regions of  $m_{B'}$  in the perturbative Yukawa coupling region can be covered. Exclusions of  $m_{B'}$  up about 800 GeV could be achieved with  $10 \text{ fb}^{-1}$  integrated luminosity. Note that at the LHC, we could tolerate a much smaller  $m_{B'} - m_X$  almost up to the on-shell decay threshold for small  $m_{B'}$ . The  $3\sigma$  discovery reach for  $m_{B'}$  is about 380, 540, 700 GeV for integrated luminosities of 0.1, 1, and  $10 \text{ fb}^{-1}$ . The reach in  $m_X$  is greatly enhanced at the LHC as well. It could be excluded up to 330 and 410 GeV, or to be discovered up to 260 and 360 GeV with 1 and  $10 \text{ fb}^{-1}$  data.

Note that the exclusion curve for the Tevatron in Fig. 3 fails to reach the  $m_X = m_{B'} - m_b$  line for any values of  $m_{B'}$ , because of the small missing energy in this region. As evident in

<sup>2</sup> By Gaussian equivalent, we mean that we have converted the one-sided Poisson probability into the equivalent  $\sigma$  deviation in a two-sided Gaussian distribution, which is more commonly used in the literature.

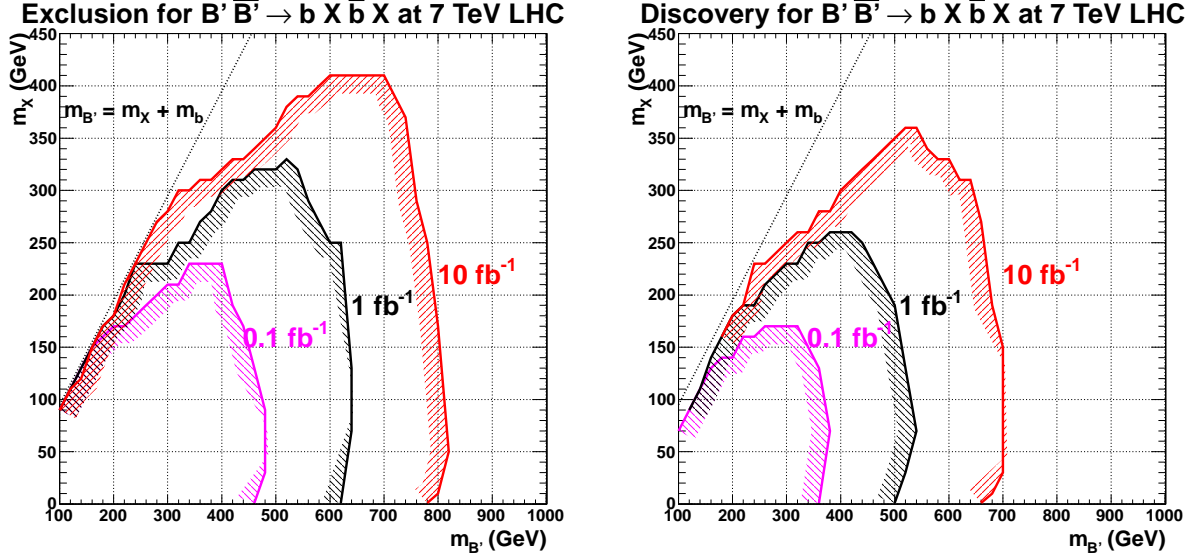


FIG. 4: 95% CL LHC 7 TeV exclusion (left plot) and  $3\sigma$  discovery (right plot) reach in the  $(m_{B'}, m_X)$  plane for integrated luminosities 0.1, 1, and  $10 \text{ fb}^{-1}$ . For each point in parameter space, the cut with the best significance has been chosen.

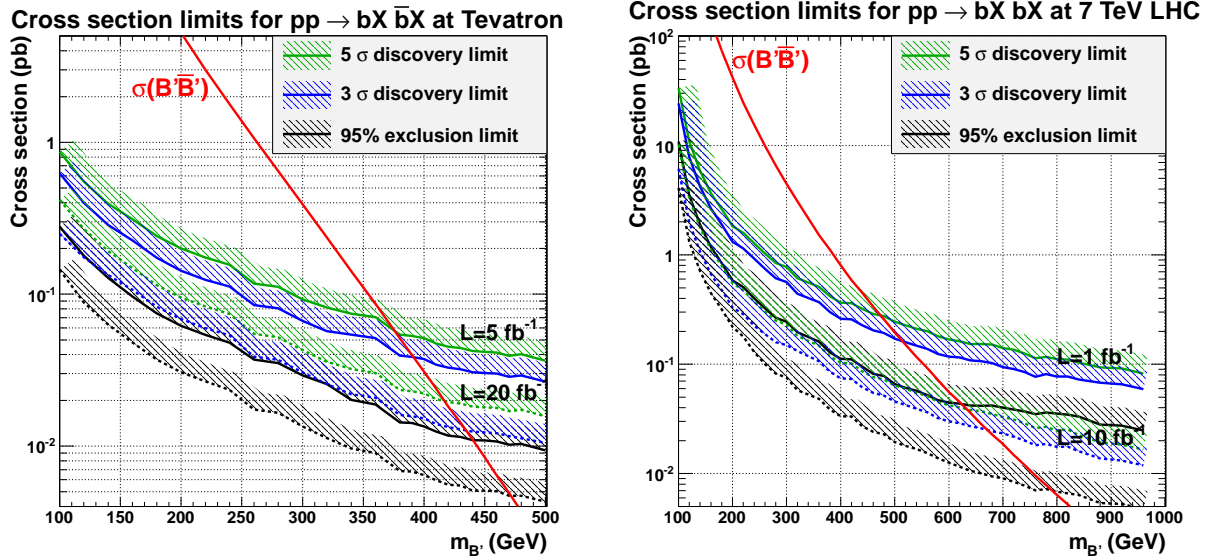


FIG. 5: Model-independent 95% exclusion,  $3\sigma$  and  $5\sigma$  discovery cross section reaches for light  $m_X$  ( $m_X = 1 \text{ GeV}$ ) at the Tevatron (left plot) and 7 TeV LHC (right plot). Also shown are the QCD pair production cross sections for  $B'\bar{B}'$  (solid red curves).

Fig. 4, however, this is not true at the LHC, where the energy and cross section for low-mass  $B'$ 's are so large that recoil of the  $B'\bar{B}'$  system against initial state radiation jets gives events with sufficient  $\cancel{E}_T$  to pass the cuts, even for  $m_X = m_{B'} - m_b$ . For further discussion, see Ref. [45].

To present our exclusion and discovery reaches in a more model-independent way, in Fig. 5 we show the collider reaches of the  $bX\bar{b}X$  production cross section [or equivalently,

$\sigma(B'\bar{B}') \times B(B' \rightarrow bX)^2]$  as a function of  $m_{B'}$  for 95% CL exclusion,  $3\sigma$  and  $5\sigma$  discovery for various luminosities at the Tevatron and the 7 TeV LHC, with  $m_X$  fixed to 1 GeV. At the Tevatron with  $20 \text{ fb}^{-1}$ , production cross sections of 5–200 fb could be excluded at 95% CL for the mass of  $B'$  in the range of 100–500 GeV. The limits get better for higher masses due to the more energetic final state particles and large  $\cancel{E}_T$  and  $M_{\text{eff}}$  in the signal process. For  $5\sigma$  discovery, the cross section reach is about 20–400 fb. At the 7 TeV LHC, with  $1 \text{ fb}^{-1}$  luminosity we could reach an exclusion limit of about 25 fb for  $m_{B'}$  around 1 TeV. A  $5\sigma$  reach of 20 fb can be achieved with  $10 \text{ fb}^{-1}$  luminosity.

For the purpose of illustration, we also show the QCD pair production cross sections of  $B'\bar{B}'$  (solid curves) in Fig. 5. For  $B'\bar{B}'$  pair production in other new physics models, one can easily read out the collider reach of  $m_{B'}$  by comparing  $\sigma(B'\bar{B}') \times B(B' \rightarrow bX)^2$  in those models with the cross section reach curves in Fig. 5.

Note that we have taken  $m_X = 1 \text{ GeV}$  when presenting the cross section reaches at colliders. However, as evident from Figs. 3 and 4, the reach in  $m_{B'}$  is almost independent of  $m_X$  for small and moderate values of  $m_X$ , unless the mass splitting of  $m_{B'} - m_X$  becomes small.

## VI. CONCLUSIONS

In this study, we have considered the possibility of pair production of new charge  $-\frac{1}{3}$  quarks  $B'$  that decay directly to  $b$ -quarks and long-lived neutral particles  $X$ . The resulting signal is  $B'\bar{B}' \rightarrow b\bar{b}\cancel{E}_T$ , which is common to many new physics theories, as discussed in Sec. II. Since the  $b\bar{b}\cancel{E}_T$  signal is common to many models, we have also presented detection prospects in terms of the pair production cross-section  $\sigma(b\bar{b}XX)$ , for varying  $m_{B'}$  and various integrated luminosities. This analysis thus accommodates many models in which there are new contributions to  $B'\bar{B}'$  production, as well as models where  $B'$  is not spin- $\frac{1}{2}$ , as in the case of bottom squarks.<sup>3</sup>

We have estimated the sensitivity of the Tevatron and LHC to new physics resulting in this signal. Currently published bounds have been summarized in detail in Sec. III; very roughly, however, and translating bounds on related processes to the case of  $B'\bar{B}'$  production, the current limits are  $m_{B'} \gtrsim 370 \text{ GeV}$ . From our analysis, we expect that these results may be improved to  $m_{B'} \gtrsim 440 \text{ GeV}$  for small  $m_X$ , given our optimized cuts and  $5 \text{ fb}^{-1}$  of data, which is currently available at the Tevatron. We also find that additional Tevatron data will marginally improve this bound: for  $20 \text{ fb}^{-1}$  of data, models with  $m_{B'} \leq 480 \text{ GeV}$  ( $m_X \lesssim 150 \text{ GeV}$ ) can be excluded at 95% CL.

These results may be further improved at the LHC with an analysis of  $1 \text{ fb}^{-1}$  of data, which has already been accumulated. With  $1 \text{ fb}^{-1}$  of integrated luminosity, the LHC physics run can probe any models with  $m_{B'} \lesssim 620 \text{ GeV}$ , provided  $m_X \lesssim 250 \text{ GeV}$ . Models with  $B'$  quarks that get mass from electroweak symmetry breaking are bounded by the requirement of perturbative Yukawa couplings to have masses below this mass. Early LHC data may therefore probe the full range of possible quark masses in these models. In particular, the early LHC will probe all WIMPless models that could explain the data of DAMA and CoGeNT (assuming dominant coupling to 3rd generation SM quarks). Even null results

<sup>3</sup> If  $B'$  is not spin- $\frac{1}{2}$ , then the angular distributions of the outgoing jets will change, altering cut efficiencies.

In this case, the comparison is only approximate.

from the search discussed here will therefore be of significant interest.

These same detection prospects are, of course, also applicable to little Higgs models, or asymmetric dark matter models arising from hidden sector baryogenesis. For these models, however, theoretical considerations provide no expected upper bound on  $m_{B'}$ . The mass reach which the LHC can achieve with greater luminosity is thus of interest. With  $10 \text{ fb}^{-1}$  of data, the LHC can probe asymmetric dark matter models and other similar frameworks at the 95% CL for  $m_{B'} \lesssim 800 \text{ GeV}$ , provided  $m_X \lesssim 200 \text{ GeV}$ .

UED models have perhaps the least constrained theoretical motivation, since the  $B'$  mass is not bounded by Yukawa coupling perturbativity and relatively small  $B' - X$  mass splittings are perfectly plausible. With  $10 \text{ fb}^{-1}$  the LHC can probe models with  $m_X$  as large as  $410 \text{ GeV}$  at the 95% CL. This maximum reach is obtained for  $m_{B'}$  in the  $600 - 700 \text{ GeV}$  range.

All of these detection prospects can be easily translated into mass reaches for bottom squarks decaying directly to  $b\chi_1^0$ . With  $1 \text{ fb}^{-1}$ , the LHC can probe models with  $m_{\tilde{b}} \leq 400 \text{ GeV}$  at 95% CL (provided  $m_{\chi_1^0} \lesssim 150 \text{ GeV}$ ). With  $10 \text{ fb}^{-1}$ , the LHC reach increases to  $m_{\tilde{b}} \leq 520 \text{ GeV}$ .

It is worthwhile to compare the mass reach of this  $B'$  search to that of the  $T'$  search examined in Ref. [1]. There it was found that, with  $1 \text{ fb}^{-1}$  of data, the LHC could probe low-mass dark matter models at  $3\sigma$  for  $m_{T'} \leq 490 \text{ GeV}$ . The  $B'$  search described here has similar reach for the same luminosity and required signal significance. However, the  $T'$  detection prospects were seen to drop rapidly with increasing  $m_X$ , with no sensitivity at all expected for  $m_X \geq 180 \text{ GeV}$ . In contrast, the detection prospects for this  $B'$  search are almost unchanged for  $m_X \lesssim 200 \text{ GeV}$  (assuming  $3\sigma$  significance). This difference is attributable to the large mass of the top quark; for relatively heavy  $X$ , there is very little phase space left for the  $T' \rightarrow tX$  decay. Although the  $t\bar{t}\cancel{E}_T$  signals provides many more handles, in the end, the naive expectation holds true: the reaches in  $m_{B'}$  and  $m_{T'}$  are roughly similar, and for a fixed new quark mass, the dark matter mass reach of the  $B'$  search exceeds that of the  $T'$  search by roughly  $m_t - m_b \approx 170 \text{ GeV}$ .

The analysis presented here determines the prospects for detecting an excess in events with  $b$ -jets and missing  $E_T$ . It is more difficult to determine if the excess arises from the pair production of  $B'$ , decaying via  $B' \rightarrow bX$ . To determine the masses  $m_{B'}$  and  $m_X$  would be harder still. It would be interesting to determine the prospects for the LHC to make these measurements.

## VII. ACKNOWLEDGMENTS

We are grateful to T. Tait for useful discussions. JA is supported by Fermi Research Alliance, LLC under Contract No. DE-AC02-07CH11359 with the United States Department of Energy. The work of JLF and SS was supported in part by the National Science Foundation under Grants PHY-0653656 and PHY-0970173. The work of JK was supported in part by the Department of Energy under Grant DE-FG02-04ER41291. The work of SS was supported in part by the Department of Energy under Grant DE-FG02-04ER-41298.

## Appendix: Impact of Cuts on Signal and Backgrounds

In this Appendix, we present tables listing the cross sections after cuts for the  $B'\bar{B}'$  signal and the main SM backgrounds (Tables I-II). In the upper section of each table, each line gives the cross section after including all cuts above. In the lower section, each line gives the cross section after including the cut on that line, and all precuts. For the signal, three examples with  $m_X = 1$  GeV and  $m_{B'} = 200, 300$ , and  $400$  (300, 500 and 800) GeV were chosen for the Tevatron (7 TeV LHC). The  $W$  and  $Z$  cross sections in parentheses were simulated with a cut on  $\cancel{E}_T > 20$  (60) GeV for the Tevatron (LHC) and at least 2 jets in the parton-level generation.

TABLE I: Signal and background cross sections in pb after cuts for signal and dominant backgrounds at the Tevatron. The signal examples are for  $m_X = 1$  GeV and  $m_{B'} = 200, 300$ , and  $400$  GeV as indicated. The  $W$  cross sections in parentheses were simulated with a cut on  $\cancel{E}_T > 20$  GeV and at least 2 jets in the parton-level generation. From the 160 independent combinations of final cuts used for the cut optimization, the three cuts that optimize the significance for these three mass points are displayed in the table. Momenta and masses are in GeV.

	$B'$ (200)	$B'$ (300)	$B'$ (400)	$W^\pm$ +jets	$Z \rightarrow \nu\nu$ +jets	$t\bar{t}$ +jets
No cut	2.62	0.195	0.0154	(632.45)	(21.103)	5.628
0 leptons	2.24	0.169	0.0134	(229.22)	(16.516)	2.365
$2 \leq \text{jets} \leq 3$	1.89	0.143	0.0109	(33.80)	(7.962)	0.456
$\alpha_{j_1 j_2} < 165^\circ$	1.66	0.125	0.0097	(29.35)	(7.171)	0.362
$\cancel{E}_T > 40$	1.55	0.122	0.0096	17.05	5.221	0.235
$\cancel{E}_T > 80 - 40 \times \Delta\phi_{min}^{(\cancel{E}_T, \text{jets})}$	1.52	0.121	0.0095	16.45	5.042	0.207
$\Delta\phi(\cancel{E}_T, \text{jets}) > 0.6$	1.43	0.112	0.0086	16.29	4.957	0.188
$\mathcal{A} \equiv \frac{\cancel{E}_T - H_T}{\cancel{E}_T + H_T}$ cut	1.42	0.111	0.0086	15.89	4.869	0.179
$X_{jj} \equiv (p_T^{j_1} + p_T^{j_2})/H_T > 0.75$	1.25	0.102	0.0081	13.48	4.197	0.079
$p_T^{j_1} > 20$	1.25	0.102	0.0081	13.48	4.197	0.079
$H_T > 60$	1.25	0.102	0.0081	10.56	3.680	0.078
$\geq 2$ $b$ -jets, $b$ -jet hardest jet	0.43	0.035	0.0026	0.11	0.037	0.018
All precuts	0.43	0.035	0.0026	0.11	0.037	0.018
$X_{jj} > 0.9, \cancel{E}_T > 40, H_T > 300$	0.018			$8.59 \cdot 10^{-5}$	$1.11 \cdot 10^{-4}$	$1.68 \cdot 10^{-4}$
$X_{jj} > 0.9, \cancel{E}_T > 150, H_T > 300$		0.0043		$4.56 \cdot 10^{-5}$	$7.40 \cdot 10^{-5}$	$4.11 \cdot 10^{-5}$
$X_{jj} > 0.9, \cancel{E}_T > 250, H_T > 300$			$5.30 \cdot 10^{-4}$	$1.95 \cdot 10^{-5}$	$4.02 \cdot 10^{-5}$	$1.39 \cdot 10^{-5}$

- 
- [1] J. Alwall, J. L. Feng, J. Kumar and S. Su, Phys. Rev. D **81**, 114027 (2010) [arXiv:1002.3366 [hep-ph]].
  - [2] R. Bernabei *et al.* [DAMA Collaboration], Eur. Phys. J. C **56**, 333 (2008) [arXiv:0804.2741 [astro-ph]]; Eur. Phys. J. C **67**, 39 (2010) [arXiv:1002.1028 [astro-ph.GA]].
  - [3] C. E. Aalseth *et al.* [CoGeNT Collaboration], Phys. Rev. Lett. **106**, 131301 (2011) [arXiv:1002.4703 [astro-ph.CO]]; Phys. Rev. Lett. **107**, 141301 (2011) [arXiv:1106.0650 [astro-]]

TABLE II: Signal and background cross sections in pb after cuts for signal and dominant backgrounds at 7 TeV LHC. The signal examples are for  $m_X = 1$  GeV and  $m_{B'} = 300, 500, \text{ and } 800$  GeV as indicated. The  $W$  cross sections in parentheses were simulated with a cut on  $\cancel{E}_T > 60$  GeV and at least 2 jets in the parton-level generation. From the 104 independent combinations of final cuts used for the cut optimization, the three cuts that optimize the significance for these three mass points are displayed in the table. Momenta are in GeV units.

Cut	$B'$ (300)	$B'$ (500)	$B'$ (800)	$W^\pm + \text{jets}$	$Z \rightarrow \nu\nu + \text{jets}$	$t\bar{t}$
No cuts	4.47	0.195	$6.39 \cdot 10^{-3}$	(194.13)	(49.19)	94.96
0 leptons	4.05	0.179	$5.83 \cdot 10^{-3}$	(104.32)	(43.69)	50.07
$\geq 2$ jets, $p_T^{j_1} > 100$ , veto 4th jet at 30 GeV	2.64	0.122	$3.79 \cdot 10^{-3}$	(18.50)	(12.33)	6.99
$\cancel{E}_T > 80$	2.20	0.113	$3.67 \cdot 10^{-3}$	13.55	9.77	1.66
$f \equiv \cancel{E}_T/M_{\text{eff}} > 0.3$ (2-jets)	1.75	0.090	$3.00 \cdot 10^{-3}$	9.93	7.69	1.29
$f \equiv \cancel{E}_T/M_{\text{eff}} > 0.25$ (3-jets)	1.55	0.080	$2.66 \cdot 10^{-3}$	9.30	7.37	0.94
$\Delta\phi(\cancel{E}_T, \text{jets}) > 0.2$	1.50	0.077	$2.49 \cdot 10^{-3}$	8.82	7.04	0.89
$S_T > 0.2$	0.91	0.045	$1.42 \cdot 10^{-3}$	3.79	3.21	0.52
$\geq 1$ $b$ -jet	0.53	0.026	$8.51 \cdot 10^{-4}$	0.21	0.22	0.26
All precuts	0.53	0.026	$8.51 \cdot 10^{-4}$	0.21	0.22	0.26
$p_T^{j_1} > 100, \cancel{E}_T > 80, M_{\text{eff}} > 600$	0.101			$6.6 \cdot 10^{-3}$	0.012	$4.0 \cdot 10^{-3}$
$p_T^{j_1} > 250, \cancel{E}_T > 300, M_{\text{eff}} > 700$		0.010		$1.0 \cdot 10^{-3}$	$2.4 \cdot 10^{-3}$	$1.5 \cdot 10^{-4}$
$p_T^{j_1} > 400, \cancel{E}_T > 80, M_{\text{eff}} > 400$			$4.7 \cdot 10^{-4}$	$1.6 \cdot 10^{-4}$	$3.7 \cdot 10^{-4}$	$5.08 \cdot 10^{-5}$

ph.CO]].

- [4] See talk of W. Seidel at IDM2010, <http://indico.in2p3.fr/contributionDisplay.py?contribId=195&sessionId=9&confId=1565>.
- [5] H. Goldberg, Phys. Rev. Lett. **50**, 1419 (1983) [Erratum-ibid. **103**, 099905 (2009)].
- [6] J. R. Ellis, J. S. Hagelin, D. V. Nanopoulos, K. A. Olive and M. Srednicki, Nucl. Phys. B **238**, 453 (1984).
- [7] K. Nakamura *et al.* [Particle Data Group Collaboration], J. Phys. G **G37**, 075021 (2010).
- [8] G. Servant and T. M. P. Tait, Nucl. Phys. B **650**, 391 (2003) [arXiv:hep-ph/0206071].
- [9] H. C. Cheng, J. L. Feng and K. T. Matchev, Phys. Rev. Lett. **89**, 211301 (2002) [arXiv:hep-ph/0207125].
- [10] J. L. Feng and J. Kumar, Phys. Rev. Lett. **101**, 231301 (2008) [arXiv:0803.4196 [hep-ph]]; J. L. Feng, H. Tu and H. B. Yu, JCAP **0810**, 043 (2008) [arXiv:0808.2318 [hep-ph]]; J. L. Feng, M. Kaplinghat, H. Tu and H. B. Yu, JCAP **0907**, 004 (2009) [arXiv:0905.3039 [hep-ph]]; J. L. Feng and Y. Shadmi, Phys. Rev. D **83**, 095011 (2011) [arXiv:1102.0282 [hep-ph]].
- [11] J. L. Feng, J. Kumar, D. Marfatia and D. Sanford, Phys. Lett. B **703**, 124 (2011) [arXiv:1102.4331 [hep-ph]].
- [12] J. L. Feng, J. Kumar and L. E. Strigari, Phys. Lett. B **670**, 37 (2008) [arXiv:0806.3746 [hep-ph]]; G. Zhu, Phys. Rev. D **83**, 076011 (2011) [arXiv:1101.4387 [hep-ph]].
- [13] V. M. Abazov *et al.* [D0 Collaboration], Phys. Lett. B **693**, 95 (2010) [arXiv:1005.2222 [hep-ex]].
- [14] T. Aaltonen *et al.* [CDF Collaboration], Phys. Rev. Lett. **105**, 081802 (2010) [arXiv:1005.3600 [hep-ex]].

- [15] T. Aaltonen *et al.* [CDF Collaboration], Phys. Rev. Lett. **102**, 221801 (2009) [arXiv:0903.2618 [hep-ex]].
- [16] D. S. Akerib *et al.* [CDMS Collaboration], Phys. Rev. **D82**, 122004 (2010) [arXiv:1010.4290 [astro-ph.CO]]; Z. Ahmed *et al.* [CDMS-II Collaboration], Phys. Rev. Lett. **106**, 131302 (2011) [arXiv:1011.2482 [astro-ph.CO]].
- [17] E. Aprile *et al.* [XENON100 Collaboration], arXiv:1104.2549 [astro-ph.CO]; J. Angle *et al.* [XENON10 Collaboration], Phys. Rev. Lett. **107**, 051301 (2011) [arXiv:1104.3088 [astro-ph.CO]].
- [18] H. C. Cheng and I. Low, JHEP **0408**, 061 (2004) [arXiv:hep-ph/0405243].
- [19] P. Fileviez Perez, M. B. Wise, Phys. Rev. **D82**, 011901 (2010) [arXiv:1002.1754 [hep-ph]]; T. R. Dulaney, P. Fileviez Perez, M. B. Wise, Phys. Rev. **D83**, 023520 (2011) [arXiv:1005.0617 [hep-ph]].
- [20] B. Dutta and J. Kumar, Phys. Lett. B **699**, 364 (2011) [arXiv:1012.1341 [hep-ph]].
- [21] B. Dutta and J. Kumar, Phys. Lett. B **643**, 284 (2006) [arXiv:hep-th/0608188].
- [22] T. Aaltonen *et al.* [CDF Collaboration], Phys. Rev. Lett. **104**, 091801 (2010) [arXiv:0912.1057 [hep-ex]].
- [23] T. Aaltonen *et al.* [CDF Collaboration], Phys. Rev. Lett. **106**, 141803 (2011) [arXiv:1101.5728 [hep-ex]].
- [24] CDF Collaboration, CDF/PUB/TOP/PUBLIC/10395,  
[http://www-cdf.fnal.gov/physics/new/top/2011/search\\_tprime/public\\_5.6.html](http://www-cdf.fnal.gov/physics/new/top/2011/search_tprime/public_5.6.html).
- [25] DØ Collaboration, DØ Note 5892-CONF.
- [26] S. Chatrchyan *et al.* [CMS Collaboration], Phys. Lett. B **701**, 204 (2011) [arXiv:1102.4746 [hep-ex]].
- [27] ATLAS Collaboration, ATLAS-CONF-2011-022.
- [28] G. Aad *et al.* [ATLAS Collaboration], Phys. Lett. B **701**, 398 (2011) [arXiv:1103.4344 [hep-ex]].
- [29] H. J. He, N. Polonsky and S. f. Su, Phys. Rev. D **64**, 053004 (2001) [arXiv:hep-ph/0102144]; J. Alwall *et al.*, Eur. Phys. J. C **49**, 791 (2007) [arXiv:hep-ph/0607115]; G. D. Kribs, T. Plehn, M. Spannowsky and T. M. P. Tait, Phys. Rev. D **76**, 075016 (2007) [arXiv:0706.3718 [hep-ph]]; R. Fok and G. D. Kribs, Phys. Rev. D **78**, 075023 (2008) [arXiv:0803.4207 [hep-ph]]; B. Holdom, W. S. Hou, T. Hurth, M. L. Mangano, S. Sultansoy and G. Unel, PMC Phys. A **3**, 4 (2009) [arXiv:0904.4698 [hep-ph]]; M. Hashimoto, Phys. Rev. D **81**, 075023 (2010) [arXiv:1001.4335 [hep-ph]].
- [30] T. Aaltonen *et al.* [CDF Collaboration], Phys. Rev. Lett. **106**, 191801 (2011) [arXiv:1103.2482 [hep-ex]].
- [31] T. Aaltonen *et al.* [CDF Collaboration], Phys. Rev. D **82**, 092001 (2010) [arXiv:1009.0266 [hep-ex]].
- [32] V. M. Abazov *et al.* [D0 Collaboration], Phys. Lett. B **675**, 289 (2009) [arXiv:0811.0459 [hep-ex]].
- [33] A. G. Ivanov [CDF Collaboration], arXiv:0811.0788 [hep-ex].
- [34] ATLAS Collaboration, ATLAS-CONF-2011-036.
- [35] J. Alwall *et al.*, JHEP **0709**, 028 (2007) [arXiv:0706.2334 [hep-ph]].
- [36] T. Sjostrand, S. Mrenna and P. Skands, JHEP **0605**, 026 (2006) [arXiv:hep-ph/0603175].
- [37] J. Pumplin, D. R. Stump, J. Huston, H. L. Lai, P. M. Nadolsky and W. K. Tung, JHEP **0207**, 012 (2002) [arXiv:hep-ph/0201195].
- [38] PGS – Pretty Good Simulator, <http://www.physics.ucdavis.edu/~conway/research/software/>

- pgs/pgs4-general.html.
- [39] V. M. Abazov *et al.* [D0 Collaboration], Phys. Lett. B **693**, 95 (2010) [arXiv:1005.2222 [hep-ex]].
  - [40] ATLAS Collaboration, ATLAS-CONF-2010-065; ATLAS-CONF-2010-079; ATL-PHYS-PUB-2010-010.
  - [41] ATLAS Collaboration, ATL-PHYS-PUB-2009-084.
  - [42] G. Aad *et al.* [ATLAS Collaboration], arXiv:0901.0512 [hep-ex].
  - [43] J. M. Campbell, R. K. Ellis, Phys. Rev. **D65**, 113007 (2002) [hep-ph/0202176].
  - [44] M. Cacciari, S. Frixione, M. L. Mangano, P. Nason, G. Ridolfi, JHEP **0809**, 127 (2008) [arXiv:0804.2800 [hep-ph]].
  - [45] J. Alwall, M. -P. Le, M. Lisanti, J. G. Wacker, Phys. Lett. **B666**, 34-37 (2008) [arXiv:0803.0019 [hep-ph]].